RAPID COMMUNICATIONS IN MASS SPECTROMETRY
Rapid Commun. Mass Spectrom. 2007; **21**: 2157–2166
Published online in Wiley InterScience (www.interscience.wiley.com) DOI: 10.1002/rcm.3078

Laser desorption/ionization mass spectrometry on porous silicon for metabolome analyses: influence of surface oxidation

Seetharaman Vaidyanathan[1*,†], Dan Jones[3], Joanne Ellis[1], Tudor Jenkins[3], Chin Chong[2], Mike Anderson[2] and Royston Goodacre[1]

[1]School of Chemistry, Manchester Interdisciplinary Biocentre, The University of Manchester, 131, Princess Street, Manchester M1 7DN, UK
[2]School of Chemistry, The University of Manchester, Oxford Road, Manchester M13 9LP, UK
[3]Institute of Physical and Mathematical Sciences, University of Wales, Aberystwyth, Ceredigion SY23 3BZ, UK

Received 21 December 2006; Revised 4 April 2007; Accepted 1 May 2007

Laser desorption/ionization mass spectrometry (LDI-MS) on porous silicon is a promising analytical strategy for the rapid detection of metabolites in biological matrices. We show that both oxidized and unoxidized porous silicon surfaces are useful in detecting protonated/deprotonated molecules from compounds when analyzed in mixtures. We demonstrate the feasibility of using this technique for the simultaneous detection of multiple analytes using a synthetic cocktail of 30 compounds commonly associated with prokaryotic and eukaryotic primary metabolism. The predominantly detected species were the protonated molecules or their sodium/potassium adducts in the positive-ion mode and the deprotonated molecules in the negative-ion mode, as opposed to fragments or other adducts. Surface oxidation appears to influence mass spectral responses; in particular, in the mixture we studied, the signal intensities of the hydrophobic amino acids were noticeably reduced. We show that whilst quantitative changes in individual analytes can be detected, ion suppression effects interfere when analyte levels are altered significantly. However, the response of most analytes was relatively unaffected by changes in the concentration of one of the analytes, so long as it was not allowed to dominate the mixture, which may limit the dynamic range of this approach. The differences in the response of the analytes when analyzed in mixtures could not be accounted for by considering their gas-phase and aqueous basicities alone. The implications of these findings in using the technique for metabolome analyses are discussed. Copyright © 2007 John Wiley & Sons, Ltd.

There is an increasing realization that analyses characterizing the metabolome (intermediates of metabolism generally considered to be small molecular weight species) have a significant role in functional genomic investigations, and in turn in our understanding of biological systems.[1–5] These analyses typically involve large-scale high-throughput screening of many analytes simultaneously, and include determining changes (ideally quantitatively) in the metabolite profiles of the intracellular[6] and extracellular[7,8] matrices. To fulfill these requirements several approaches are being investigated,[5,9,10] including methods based on hyphenated techniques, such as chromatographic (GC,[11] LC[12]) or electrophoretic (CE)[6,13] separations followed by mass spectrometry. Other techniques being studied for the purpose include two-dimensional (2D) thin-layer chromatography,[14] NMR spectroscopy[15] and vibrational spectroscopic techniques including Fourier transform infrared (FT-IR) and Raman spectroscopies.[16]

An ideal requirement for profiling on a metabolome scale is to keep the sample processing steps minimal and develop simple and rational protocols, not only for ease of operation when dealing with many samples, but also because this will minimize sample intervention (e.g., no chemical derivatization needed) and keep the analysis times within manageable limits for high-throughput metabolite profiling. Mass spectrometry (MS) offers the spectral resolution required for monitoring multiple analytes. Desorption/ionization mass spectrometry has been practiced in various forms over the years. In its more recent form, matrix-assisted laser desorption/ionization (MALDI)-MS is a popular technique for the analysis of large (>500 m/z) biopolymers such as peptides, proteins and oligonucleotides. Although not as popular, its application has also been extended to the detection of lower molecular weight compounds.[17] Its 'soft' ionization characteristic is attractive for detecting protonated

*Correspondence to: S. Vaidyanathan, Manchester Interdisciplinary Biocentre, The University of Manchester, 131, Princess Street, Manchester M1 7DN, UK.
E-mail: S.Vaidyanathan@manchester.ac.uk
† Present Address: School of Chemical Engineering and Analytical Sciences, Manchester Interdisciplinary Biocentre, The University of Manchester, 131 Princess Street, Manchester M1 7DN, UK.
Contract/grant sponsor: BBSRC, UK.

or deprotonated molecules in preference to fragments, commonly detected in traditional MS using other ionization methods. In addition, the propensity to generate singly charged species, better tolerance than electrospray ionization (ESI)-MS to interference from salts and buffers, and simplicity of sample preparation, makes MALDI-MS ideally suited for simultaneous, rapid, high-throughput analyses of metabolites in complex biological mixtures, such as would be encountered in metabolomic investigations.

However, the employment of an organic matrix, as is the requirement in conventional MALDI-MS, results in interference from matrix peaks in the low-mass range. To counter this problem several strategies have been investigated. These include the use of high molecular weight compounds as matrices,[18,19] derivatization of analytes,[20] and employment of post-source decay (PSD) to reduce interferences from matrix ions.[21] In addition, it has been shown that the employment of lower than conventional matrix-to-analyte molar ratios is an effective means of suppressing matrix signals.[22] However, it has also been noted that the application of the strategy to analyze multiple compounds in mixtures is limited by analyte ion suppression effects.[23]

In an alternative approach, Siuzdak and coworkers have pioneered the development of porous silicon as the substrate for 'soft' laser desorption/ionization mass spectrometry;[24–27] a technique termed desorption ionization on porous silicon (DIOS). DIOS has been shown to be effective in generating 'clean' spectra of low molecular weight compounds without complications from matrix peaks. It has also been shown that the information derived can be quantitatively interpreted.[28,29] Although the mechanism of DIOS is not entirely understood, preliminary investigations point to the importance of surface morphology. Pore size and surface porosity have been found to correlate with improved performance in DIOS,[25,30–32] as does solvent-surface wetting characteristics;[32] crystal orientation and photoluminescence do not seem to influence DIOS performance.[30,32] It has also been noted that although a porous surface *per se* is not required for laser desorption in DIOS, a thick porous layer substantially improves the analyte ion signal, possibly by resupplying the surface with analyte after a laser pulse.[33]

Porous silicon surfaces are oxidized when stored in air for extended periods of time[34] or on brief exposure to ozone[35] or aqueous hydrogen peroxide,[36] which have been reported to result in poor DIOS performance.[30] However, oxidized porous silicon surfaces have been demonstrated to be viable for the analysis of small molecules using LDIMS (desorption/ionization on porous silicon dioxide – DIOSD).[37] Among the features listed in its favour, compared with DIOS, are high chemical passivity, simpler fabrication and higher signal-to-noise. Porous silicon surfaces are hydrophobic and can be used to concentrate the analytes (from aqueous solutions) for sensitive analysis. On the other hand, porous silicon dioxide is hydrophilic and can contribute to greater surface wettablility when using polar solvents. Both surfaces have favourable features for the detection of metabolites, as would be required for metabolomic investigations. We therefore investigated desorption/ionization on porous silicon and oxidized silicon surfaces for the simultaneous detection of multiple metabolites using synthetic cocktails, and studied consistency of changes in the spectral information with changes in the analyte concentrations. We discuss our observations and the suitability of these approaches for metabolomic investigations.

EXPERIMENTAL

Materials

Two cocktails, one consisting of 30 metabolites and the other 20 metabolites, were used in the study. Cocktail A consisted of the amino acids (all in L-form, with shorthand notations – used in figures – given in parentheses) alanine (Ala), arginine (Arg), asparagine (Asn), cysteine (Cys), glutamine (Gln), glycine (Gly), histidine (His), isoleucine (Ile), leucine (Leu), lysine (Lys), methionine (Met), phenylalanine (Phe), proline (Pro), serine (Ser), threonine (Thr), valine (Val), aspartate (Asp), glutamate (Glu), tryptophan (Trp), tyrosine (Tyr), the organic acids fumarate (Fum), citrate (Cit), malate (Mal), lactate (Lac), pyruvate (Pyr), succinate (deuteriated form – d_4-succinate) (d_4-Suc), oxaloacetate (Oaa), and the metabolites 4-aminobutyric acid (Aba), putrescine (Put) and D-glucose (G). The above metabolites were present at an equimolar concentration of 50 pmol/μL each. Cocktail B consisted of the 20 amino acids, 19 of which were at 50 pmol/μL and the 20th (histidine, unless specified otherwise) varied by dilutions such that it was present in the mixture at concentrations of 1 pmol/μL to 1 μmol/μL. All the metabolites were obtained from Sigma-Aldrich (Dorset, UK), and were dissolved in distilled, deionized water (18 Mohms-cm resistivity).

Porous silicon chips

Porous silicon target chips (n-type, 100 orientation) etched in-house were used in the study. The etching conditions used for the in-house preparation were as follows: current 6 mA/cm^2 for 2 min in a mixture of hydrofluoric acid and ethanol (1:1). For the generation of oxidized layers the chip was further surface oxidized by exposure to ozone (Ozomax Ltd, Quebec, Canada) for 3 min. A commercial DIOS porous silicon target chip (Mass Consortium Inc., USA) was also used in the study to assess quantitative determinations.

Raman spectroscopy

Raman spectra were collected using a 2000 Raman microscope (Renishaw plc, Gloucestershire, UK), equipped with a 25 mW near-infrared (785 nm) diode laser operating at ~2 mW at the sample. Spectra were acquired in the extended range of −1100 to 1100 cm^{-1} using a 50 × objective lens from five different areas on the chip, each in six replicates.

FT-IR spectroscopy

The in-house etched silicon and silicon dioxide chips were analyzed using a Hyperion microscopic accessory, equipped with a MCT (mercury cadmium telluride) detector, attached to a Bruker Equinox 55 module FT-IR spectrometer (Bruker Spectrospin Ltd., Coventry, UK). Spectra were acquired over the range 4000 to 600 cm^{-1} at a resolution of 4 cm^{-1} and 64 spectra were co-added and averaged to improve the signal-to-noise ratio.

DOI: 10.1002/rcm

Atomic force microscopy (AFM)

The porous silicon and silicon dioxide chips were examined by AFM (Veeco Instruments Ltd., Cambridge, UK) using a silicon nitride probe in the contact mode.

Mass spectrometry

The metabolite cocktail (A or B) (0.5 μL) was spotted directly onto a DIOS porous silicon target chip (Mass Consortium Inc., USA) or onto the in-house etched silicon chip. The target chip was then attached to a standard stainless steel target plate using double-sided sticky conductive carbon tape (SCI, USA) and analyzed in an Axima CFR + MALDI-ToF mass spectrometer (Shimadzu Biotech, Manchester, UK), in both the positive- and negative-ion mode. A total of 150 shots were averaged for each sample in both the acquisitions, and typical spectral collection times were 2 min per sample. Each sample was analyzed at least four times (technical replicates). The DIOS chip was washed with methanol (Primar Grade) several times (typically five) and reused where required, for replicate analyses. On average, a mass accuracy of <5 ppm and a mass resolution of 4000 (FWHM) were recorded over the range monitored.

Data analysis

Raman, FT-IR and mass spectral data were imported into MATLAB (The Math Works, Natick, MA, USA) and processed for analysis. Raman and FT-IR spectra were normalized to unit count before further analysis. Principal components analysis (PCA) was performed using the NIPALS algorithm on the normalized spectra. Prior to any comparative analyses the mass spectra (in the range 100–500 *m/z*) were binned to 0.1 *m/z* and normalized to total ion counts.

RESULTS

The objective of the investigation was to study the application of laser desorption/ionization on native and surface oxidized porous silicon for detecting several metabolites (low molecular weight components of metabolism) simultaneously, as would be useful in metabolomic investigations. We have previously demonstrated that commercially available DIOS target chips can be used for the purpose.[29] Here we compare the results from in-house prepared native and oxidized porous silicon surfaces. The mass spectrum of the mixture (Fig. 1) shows spectral information pertaining to the metabolites in the protonated $[M+H]^+$, sodiated $[M+Na]^+$ or potassiated $[M+K]^+$ forms in the positive-ion mode or the deprotonated form $[M-H]^-$ in the negative-ion mode, as observed earlier with the DIOS target chips. As perhaps expected, the basic metabolites (arginine, histidine, putrescine) dominate the positive-ion spectra, whilst the acidic ones (malic acid, citric acid) dominate the negative-ion spectra.

Comparison of analyte response on native and oxidized porous silicon surfaces

The advantage of using oxidized surfaces is the stability of the surface layer. Porous silicon undergoes surface oxidation when exposed to air for longer durations, changing the surface chemical characteristics. It would be of interest to know if this change affects the signal response for the analytes, as it will have a bearing on the age of the chip used for analysis and implications for its storage conditions. Accordingly, identically prepared silicon wafers, one oxidized and the other left unoxidized, were compared.

The surface layers (prior to deposition of the sample) were characterized using FT-IR and Raman spectroscopies as well as AFM. Figure 2 shows the composite spectral information obtained from these techniques. PCA was used to extract the FT-IR and Raman spectral differences between the native and oxidized surfaces. Figure 2(A) shows a PCA scores plot obtained from the FT-IR spectral information. A majority of the variance (>95%) between the two surfaces is accounted for by the first PC. The spectral information from the native and oxidized surfaces can be seen to be clustered separately

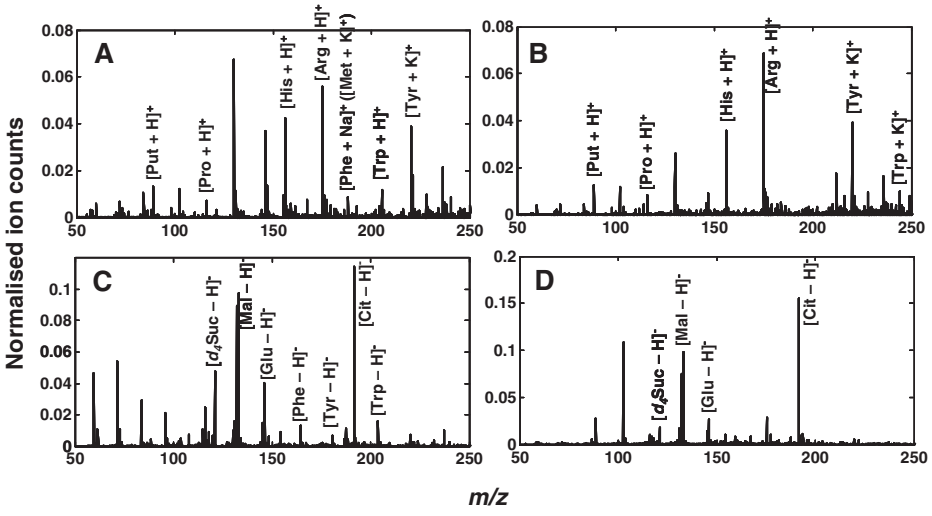

Figure 1. Typical laser desorption/ionization mass spectra of the 30-compound cocktail in the positive (A, B) and negative (C, D) ion modes, from native (A, C) and oxidized (B, D) porous silicon surfaces. Peaks corresponding to representative analytes in their protonated, deprotonated or sodium/potassium adduct forms are labeled.

DOI: 10.1002/rcm

RCM

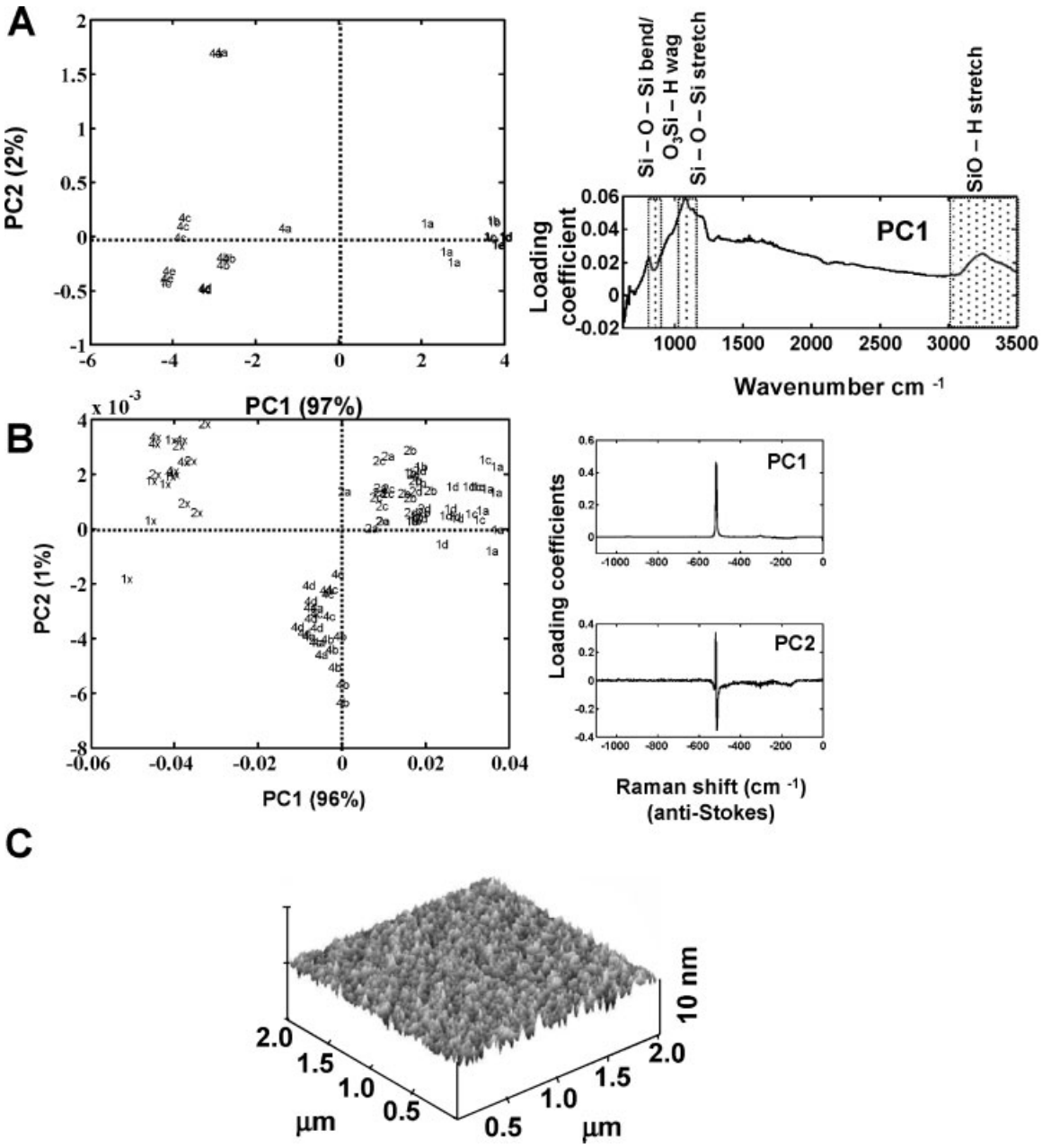

Figure 2. (A) A plot of the first two PC scores derived from the FT-IR spectra of native (1) and oxidized (4) porous silicon, acquired in different areas (a–e) within each wafer. The first PC loading is plotted alongside. The regions associated with Si-O vibrations are highlighted. (B) The PC score plot (first two PCs) derived from the Raman spectra of native (1, 2) and oxidized (4) porous silicon, acquired in different porous (a–c) and nonporous (x) areas within each wafer. The corresponding two PC loadings are plotted alongside. (C) An AFM image of the porous silicon surface showing the dimensions of the pores.

from each other indicating the difference between the two that can be monitored by FT-IR spectroscopy. Perhaps not surprisingly an inspection of the first PC loading shown alongside the scores plot in Fig. 2(A) indicates that the differences can be attributed to the bond vibrations caused by surface oxidation – the spectral intensity at the highlighted regions are higher for the oxidized wafers compared to the native ones. The prominent changes noted include those of the Si-O-Si bend at 880 cm^{-1}, the Si-O-Si asymmetric stretch at 1080 cm^{-1} and the SiO-H stretch at 3000–3650 cm^{-1}. In a similar manner, Raman spectra can also be seen to show differences between the two wafers (Fig. 2(B)). The non-porous silicon surface can be seen to cluster away from the porous surfaces, along the first PC that explains most of the variance in the data set. However, differences between the oxidized and the native surfaces emerge in the second PC. We analyzed the Raman Stokes and anti-Stokes shifts for silicon and observed that the changes in the anti-Stokes region were more useful in differentiating between the oxidation state of the wafers. Although the information in the Stokes region is mirrored in the anti-Stokes region, the strong Stokes shift at 560 cm^{-1} masks (due perhaps to saturation of signal intensity) subtle variations arising from surface differences that are modeled better in the anti-Stokes region. As can be observed from the loadings plot in Fig. 2(B), the differences between the surfaces can be attributed to changes

DOI: 10.1002/rcm

in the silicon anti-Stokes shift at $-560\,cm^{-1}$. In addition to these differences, it was also noticed that when pipetting the sample the spot beaded up when deposited on the native surface, while it did not on the oxidized surface. These observations indicate that surface oxidation has occurred on one of the surfaces, whilst the other is relatively unoxidized. Figure 2(C) shows an AFM image of the porous silicon surface that indicates surface porosity that is mesoporous in dimensions (2–50 nm).

The response of the metabolites in the mixture (cocktail A), for replicate measurements (12 in the positive- and 15 in the negative-ion mode), is shown for analysis on the oxidized (pSiO) and the native (pSi) surfaces, in the positive- (Fig. 3) and the negative- (Fig. 4) ion mode. Box-whisker plots are employed to compare the differences. The lower and upper lines of the 'box' are the 25th and the 75th percentiles of the sample; the box limits therefore indicate the interquartile range, with the horizontal bar representing the median of replicate determinations. The 'whiskers' (lines extending above and below the box) show the range (the maximum and minimum values), excluding outliers (values of >1.5 times the interquartile range). A star sign outside the whiskers

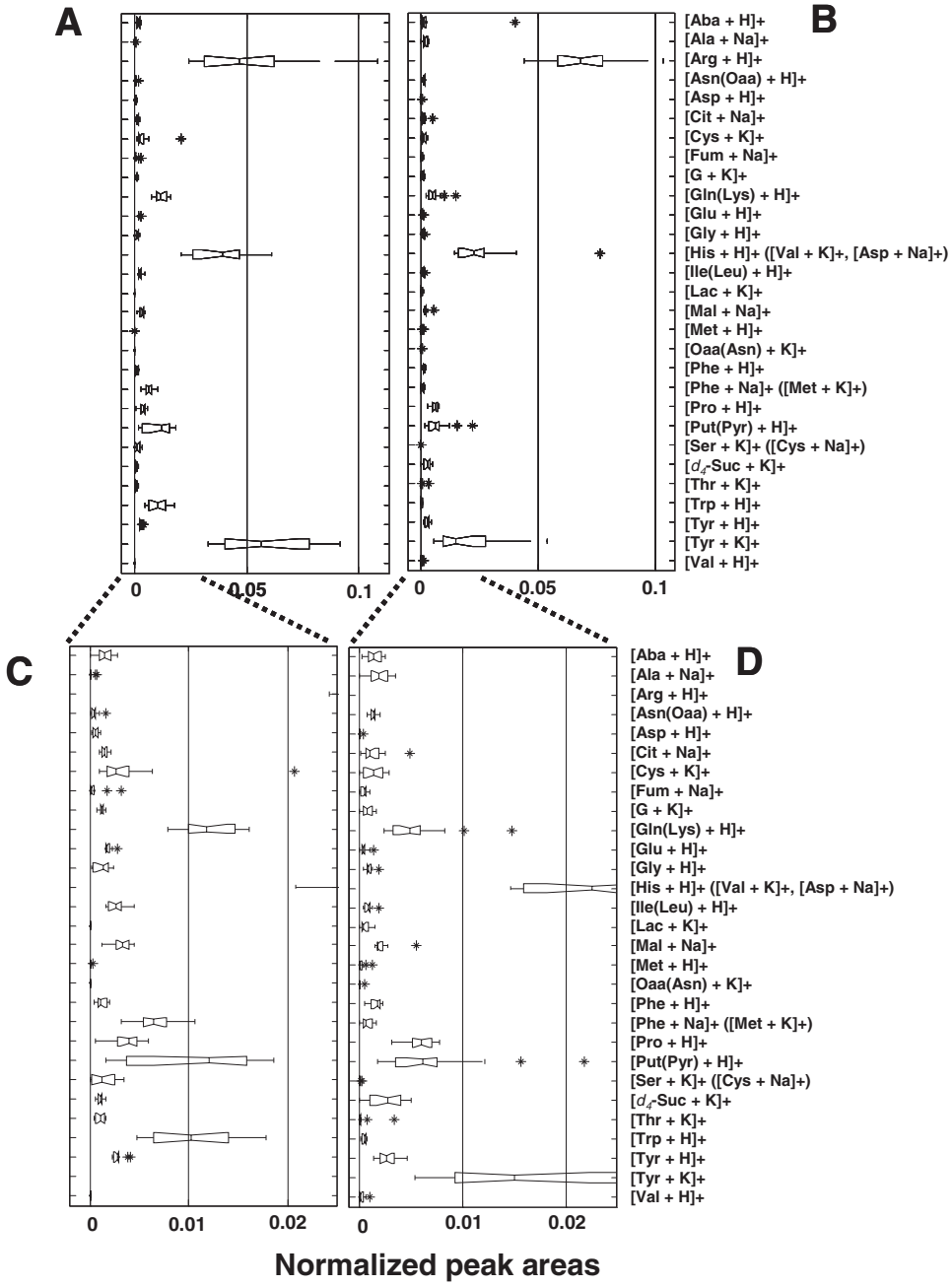

Figure 3. Comparison of the median analyte responses on native (A, C) and oxidized (B, D) porous silicon in the positive-ion mode. The response (from 12 replicate measurements) for the analytes in the mixture (cocktail A) is shown as a box-whisker plot. The low response signals can be visualized better in C and D, which contain the same information as in A and B, respectively, but zoomed in for ease of visualization.

DOI: 10.1002/rcm

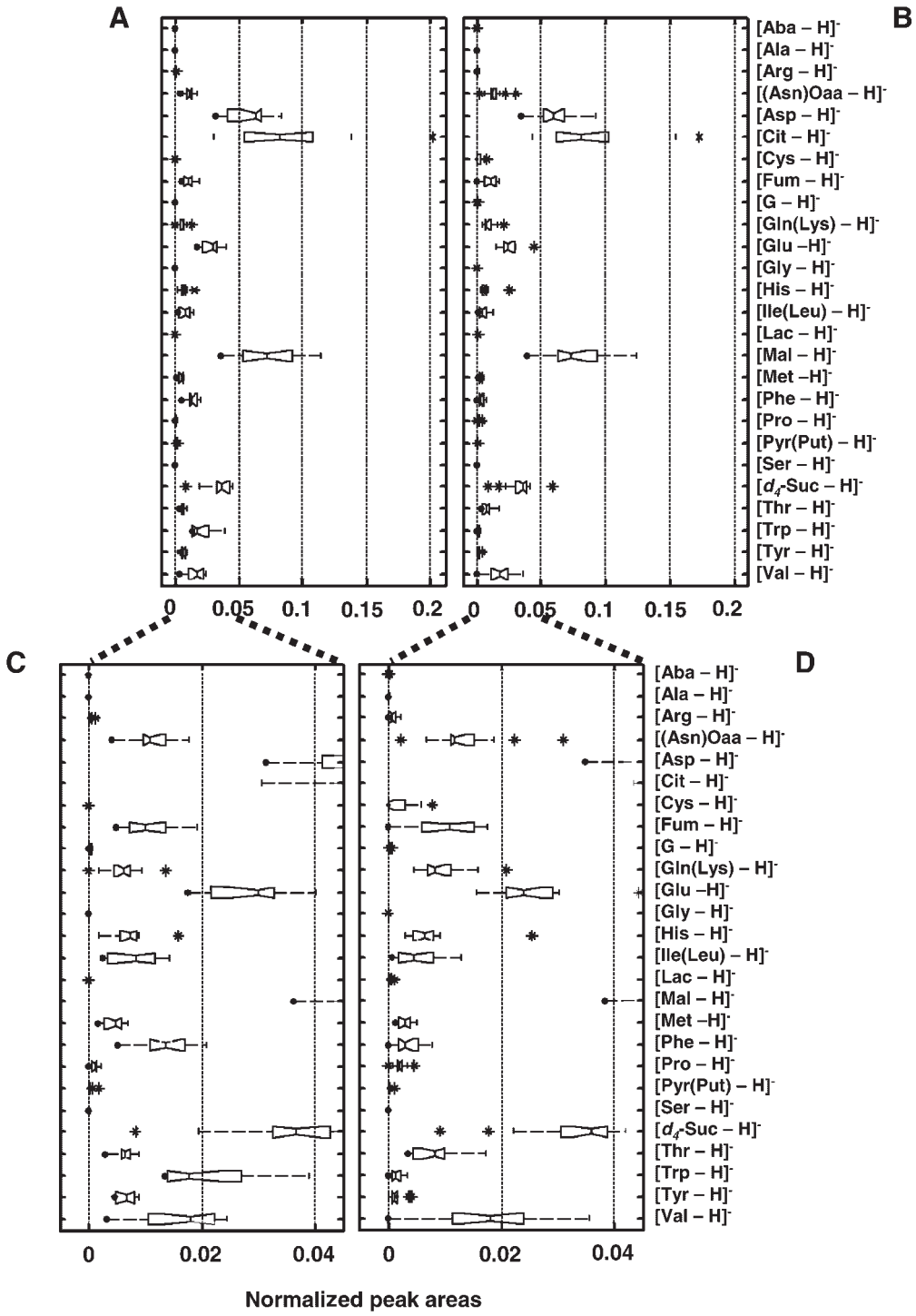

Figure 4. Comparison of the median analyte responses on native (A, C) and oxidized (B, D) porous silicon in the negative-ion mode. The response (from 15 replicate measurements) for the analytes in the mixture (cocktail A) is shown as a box-whisker plot. The low response signals can be visualized better in C and D, which contain the same information as in A and B, respectively, but zoomed in for ease of visualization.

indicates the outlier(s) in the data. The notches in the box represent a robust estimate of the uncertainty about the medians for a box to box comparison.

In the positive-ion mode, $[Arg+H]^+$ and $[Pro+H]^+$ give slightly higher signals on pSiO, as do the salt adducts $[Ala+Na]^+$, $[Glu+Na]^+$and $[d_4\text{-Suc}+K]^+$. However, $[Gln(Lys)+H]^+$, $[His+H]^+$, $[Ile(Leu)+H]^+$, $[Mal+Na]^+$, $[Phe+Na]^+$ ($[Met+K]^+$), $[Put(Pyr)+H]^+$, $[Ser+K]^+$($[Cys+Na]^+$), $[Trp+H]^+$ and $[Tyr+K]^+$ are detected more favourably on pSi. Surface oxidation appears to reduce the signals for the aromatic amino acids, tyrosine ($[Tyr+K]^+$), tryptophan ($[Trp+H]^+$) and phenylalanine ($[Phe+Na]^+$). However, the trend for the three amino acids appears to hold either for the protonated species or for one of the salt adducts and not to all three species. This is probably due to the predominance of one ionic form over the others. The observation however is clearer in the

DOI: 10.1002/rcm

negative-ion mode (Fig. 4), where only the deprotonated species is observed. Here, all the three aromatic amino acids clearly show higher signals on pSi. In addition, the hydrophobic isoleucine (leucine) ([Ile(Leu)−H]$^-$) signal is also marginally stronger on pSi, compared with pSiO, suggesting that the observed differences are due to surface hydrophobicity.

Response to changes in analyte concentrations and ion suppression effects

In addition to being able to detect multiple metabolites in a complex milieu, it is desirable to detect changes in metabolite levels in a quantitative manner. In biological systems intracellular metabolites are present not only in a complex milieu, but also at varying concentrations. It is therefore imperative that the response from the metabolites is consistent and is not overly influenced by changes in the concentration of other components in the mixture. To test this aspect, the changes in the response of the components of cocktail B were monitored, while varying the concentration of one of the components (histidine). The commercial DIOS wafer was chosen for this study. Changes in *m/z* corresponding to the protonated molecule or its sodium/potassium adduct for the 20 amino acids were monitored for each histidine spike in five replicate measurements.

The peak area at 156.2 *m/z*, corresponding to protonated histidine ([His+H]$^+$), normalized to the total ion current, is plotted in Fig. 5 as a function of the spiked concentration in three concentration ranges (0–10, 10–100 and 100–1000 pmol/μL). A proportional increase in signal intensity with increasing histidine concentrations can be seen, suggesting that the changes in a given analyte in a mixture (histidine in this study) can be captured in a quantitative manner. However, the relationship can be seen to be different at lower (0–10 and 10–100 pmol/μL) compared with the higher concentrations (100–1000 pmol/μL) of histidine spike.

The response of the other 19 analytes in the mixture to the histidine spike is summarized in Table 1, where the *p* values of the Kruskal-Wallis one-way analysis of variance (ANOVA) statistic comparing the responses for each analyte at low (<50 pmol/μL), high (>50 pmol/μL) and higher (>200 pmol/μL) histidine concentrations (the latter compared with no histidine in the mixture) are listed. As can be seen from the table, at lower histidine concentrations (<50 pmol/μL) the *p* values for most analytes suggest that there is a high probability that the median of the compared groups are the same (i.e., changes in the spiked histidine concentration do not significantly influence the mass spectral response of most analytes in the mixture). However, above 50 pmol/μL, when the concentration of the spiked analyte was increasingly higher than that of the rest, the *p* values for many analytes are closer to zero suggesting that there is a low probability that the analyte responses are the same (i.e., there may be differences in the response of the analytes to the spiked histidine). Inspecting the responses suggests suppression of response for most of the analytes (data not shown). This was pronounced for the molecular ions of proline, [Pro+H]$^+$ and [Gln(Lys)+H]$^+$, where the decrease in the respective ion responses were more-or-less proportional to the increase in the histidine concentration. However, the suppression was not as pronounced for some of the other metabolites. The differences in response for these metabolites, at higher histidine concentrations, do not seem to be significantly different from variations between replicate measurements. For example, arginine ([Arg+H]$^+$) appears to be relatively stable to changes in histidine concentrations throughout, even in the mixture that contains 20 times more histidine than arginine.

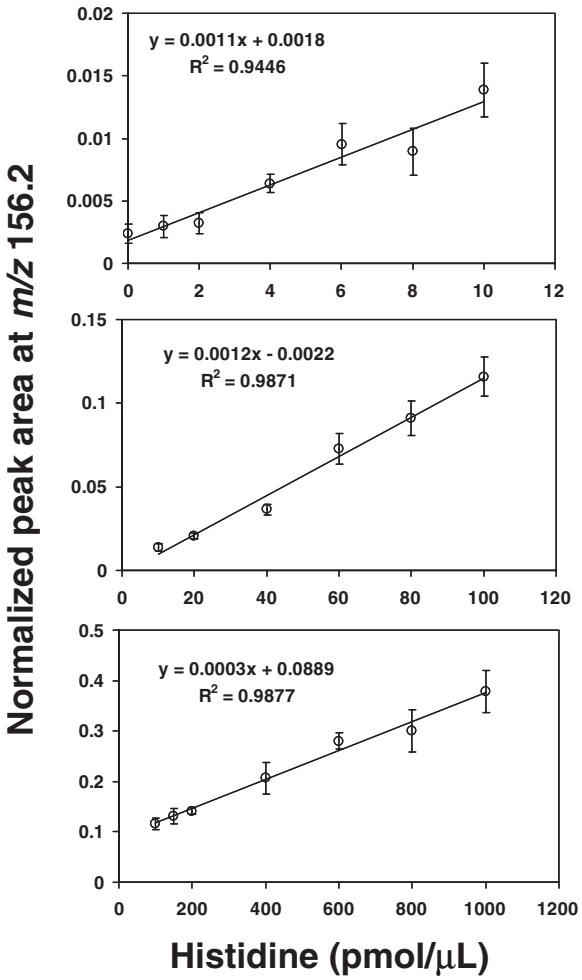

Figure 5. Changes in mass spectral response of protonated histidine in the mixture (peak area at *m/z* 156.2 normalized to total ion counts) with the spiked histidine concentration, over three different concentration ranges, showing linearity of the relationship.

DISCUSSION

Development of methods for the rapid detection and quantification of metabolites in biological matrices, using simple and rational protocols, is a significant pursuit in the post-genome era. Such an approach enables high-throughput screening of biological samples for rapid assessment of biochemical/physiological status, and in a clinical context has the potential for disease diagnosis, within realistic times (minutes rather than days or weeks). LDI-MS on porous silicon offers the means for developing analytical strategies towards such ends. The possibility of detecting molecular ions with minimal fragmentation, thanks to so-called 'soft'

DOI: 10.1002/rcm

Table 1. Influence of changes in histidine concentration on the mass spectral response of the other analytes in the mixture. The Kruskal-Wallis statistics (p >chisq) for the metabolite species (as protonated, sodium or potassium adducts) are listed for the cases where the spiked histidine concentration was (a) below the concentration of the other analytes (i.e., <50 pmol/μL), (b) above the concentration of the other analytes (>50 pmol/μL), and (c) higher (>200 pmol/μL) as compared with no spiked histidine. Contributions from more than a single species at a given *m/z* are indicated in parentheses

Metabolite species	*m/z*	Low spiked His (0–40 pmol/nL)	High spiked His (60–1000 pmol/(iL)	Higher spiked His compared to initial (0 & 200–1000 pmol/nL)
$[Ala+H]^+$	90.1	0.576	0.004	0.086
$[Ala+Na]^+$	112.1	0.635	0.673	0.621
$[Arg+H]^+$	175.2	0.170	0.305	0.541
$[Arg+Na]^+$	197.2	0.995	0.460	0.852
$[Asn+H]^+$	133.1	0.457	0.314	0.030
$[Asn+K]^+$	171.2	0.210	0.001	0.001
$[Asn+Na]^+$	155.1	0.668	0.001	0.049
$[Asp+K]^+$ ($[Met+Na]^+$)	172.2	0.810	0.020	0.388
$[Cys+K]^+$	160.3	0.892	0.037	0.454
$[Gln+H]^+$($[Lys+H]^+$)	147.2	0.235	0.000	0.000
$[Gln+K]^+$($[Lys+K]^+$)	185.2	0.014	0.019	0.004
$[Gln+Na]^+$($[Lys+Na]^+$)	169.2	0.630	0.005	0.003
$[Glu+H]^+$	148.1	0.281	0.001	0.017
$[Glu+K]^+$	186.2	0.645	0.001	0.054
$[Glu+Na]^+$	170.1	0.018	0.014	0.001
$[Gly+Na]^+$	98.1	0.426	0.022	0.070
$[Gly+K]^+$	114.2	0.470	0.469	0.504
$[Ile+H]^+$($[Leu+H]^+$)	132.2	0.109	0.694	0.033
$[Ile+Na]^+$($[Leu+Na]^+$, $[Pro+K]^+$)	154.2	0.128	0.008	0.005
$[Met+H]^+$	150.2	0.143	0.012	0.003
$[Phe+H]^+$	166.2	0.355	0.147	0.015
$[Phe+Na]^+$($[Met+K]^+$)	188.2	0.951	0.010	0.040
$[Pro+H]^+$	116.1	0.602	0.000	0.001
$[Ser+H]^+$	106.1	0.577	0.016	0.139
$[Ser+K]^+$($[Cys+Na]^+$)	144.2	0.188	0.003	0.944
$[Ser+Na]^+$($[Ala+K]^+$)	128.1	0.233	0.242	0.023
$[Thr+K]^+$	158.2	0.367	0.838	0.867
$[Thr+Na]^+$	142.1	0.983	0.026	0.046
$[Trp+H]^+$	205.2	0.247	0.002	0.327
$[Trp+K]^+$	243.3	0.081	0.001	0.431
$[Tyr+H]^+$	182.2	0.126	0.001	0.686
$[Val+H]^+$	118.2	0.336	0.127	0.020
$[Val+Na]^+$	140.1	0.837	0.777	0.366

ionization, should make it easier to detect multiple analytes with minimal information overlap. This would enable the application of the technique to metabolomic investigations where changes in multiple metabolites can be simultaneously monitored.

We studied the application of LDI-MS on porous silicon for the detection of multiple analytes using a synthetic cocktail of 30 compounds. We were primarily interested in the detection of the compounds as the protonated/deprotonated or sodium/potassium adducts, as this would simplify spectral interpretations and enable less ambiguous peak assignments, compared to fragments commonly encountered in traditional mass spectrometry with 'harder' ionization methods, such as electron impact.

The compounds could be detected as the protonated/deprotonated molecules or their sodium/potassium adducts using both oxidized and native porous silicon surfaces (Figs. 1, 3 and 4). However, surface oxidation of porous silicon appears to influence analyte responses, in particular the hydrophobic amino acids, whose signal intensities are noticeably reduced (Figs. 3 and 4). The differences appear to be due to variations in the wettability of the surface, induced by oxidation, as these would contribute to differences in the density of the analyte ions distributed on the two surfaces. Whilst this has implications with respect to the age of the surface and its storage, it suggests that such surface differences offer an additional dimension in devising strategies for analyzing multiple metabolites. Indeed, as noted by Siuzdak and coworkers,[38] the surface could be silylated not only to improve surface stability to oxidation and hydrolysis, but also to enable preparation of modified surfaces to suit analyte-specific applications or as a means for discriminating analyte responses through selective analyte adsorption.

A noticeable feature of the analyte responses on porous silicon, surface-oxidized or otherwise, is their variations for different compounds, even when all the compounds are present in equimolar concentrations (Figs. 1, 3 and 4). As is well known in such analyses, ion suppression effects are operational and there appears to be preferential formation of

DOI: 10.1002/rcm

ions. Although the mechanistic details of LDI-MS on porous silicon are not well understood, desorption and ionization are two stages where the differences can arise. It has been suggested that desorption is induced by local surface heating.[24] This is supported by the observation that unlike MALDI energy transfer in DIOS is independent of laser fluence,[39] and that irrespective of the laser fluence a surface temperature of ~800 K is required for the emission of preformed ions to occur.[33] At these temperatures most organics are either desorbed intact or decomposed to fragments. It has been noted that the internal energy transfer associated with the desorption step is fairly reproducible in DIOS suggesting stable fragment ion yields.[39] Whilst differences in the response of the compounds when analyzed individually can have a contribution from the desorption event, the relative suppression of the signals when the compounds are analyzed in a mixture appears to be due mostly to the ionization processes.

Ionization can result from chemical reactions between the silicon substrate and the analyte, from photochemical reactions between solvent trapped in pores and analyte molecules, or from gas-phase reactions. It is also possible that preformed ions and ion pairs in the condensed phase contribute to the ions detected. Apart from these, interfacial reactions accompanying desorption/ionisation[40] can also contribute. In the positive-ion mode, the detection of sodium and potassium adducts possibly originates from trace amounts of these ions in the aqueous environment in which the compounds were deposited. The detection of protonated species in desorption/ionization mass spectrometry, such as in FAB[41] and MALDI,[42] in the positive-ion mode is usually attributed to the analyte gas-phase basicities. However, it has been noted that in determining whether protonated analyte ions will be formed from porous silicon surfaces, the *aqueous* phase basicity is more important than the gas-phase basicity,[33] suggesting that competition for protons occurs in a 'wet' environment. It has been argued[33] that the solvation environment experienced by the ions between laser pulses, more than the environment at the point of desorption, determines which molecules are protonated on the surface and end up being detected.

A plot of the analyte response in the positive-ion mode as a function of their gas-phase (proton affinities – PA)[43] and aqueous basicities (pK_a) is shown in Fig. 6, for selected compounds when analyzed in cocktail A. The size of the points indicates the relative intensity of the response. Whilst arginine (coded as 2) and histidine (4) have a response that is in proportion to their gas-phase and aqueous basicities, putrescine (1) and lysine (3) show relatively poor response that is not quite proportional to their high basicities (gas-phase or aqueous). Lysine shows a disproportionately poor response even when analyzed individually. The relationship between gas-phase or aqueous basicity and mass spectral response for glutamine in a mixture fits the trend seen with the others, better than lysine. This is in accordance with the observation that glutamine gives a relatively higher response than lysine when analyzed individually in the positive-ion mode, and that the PSD spectrum of the peak at *m/z* 147 (data not shown) in the positive-ion mode spectrum resembles glutamine better,

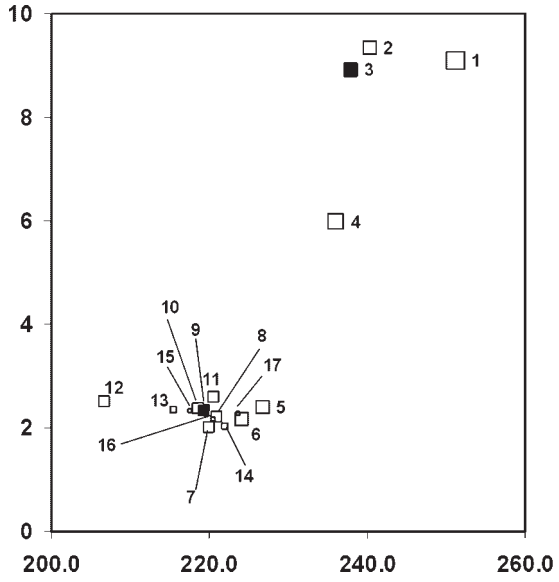

Figure 6. Analyte responses (in the positive-ion mode) as a function of gas-phase and aqueous basicities (proton affinities[43] and pK_a, respectively), when analyzed in cocktail A. Responses with closed squares indicate cases where the signal has contributions from two compounds and could be attributed better to the other compound. The size of each point indicates the relative mass spectral response (on a logarithmic scale), at the *m/z* corresponding to the protonated molecule of the compound: 1, putrescine; 2, arginine; 3, lysine (glutamine); 4, histidine; 5, tryptophan; 6, glutamine; 7, proline; 8, tyrosine; 9, isoleucine (leucine); 10, leucine; 11, phenylalanine; 12, 4-aminobutyric acid; 13, alanine; 14, asparagine; 15, valine; 16, threonine; 17, methionine.

suggesting that glutamine contributes mainly to the response at *m/z* 147.

The dramatic decrease in response of most compounds when analyzed in a mixture (e.g., alanine, leucine (isoleucine), proline, tyrosine, threonine and valine) can be accounted for based on their PA. Arginine, histidine, putrescine, glutamine and tryptophan all have relatively higher PA that enables them to abstract available protons more readily than the rest; hence the latter's poor or suppressed response. Many of the compounds show similar aqueous basicities yet different mass spectral responses. For instance, 4-aminobenzoic acid has a similar aqueous basicity as valine, threonine and methionine, but it shows a relatively good response, despite having the lowest gas-phase basicity, whilst the responses of the other three are completely suppressed. Proline shows a relatively good response even though its aqueous basicity is the least. Clearly for LDI-MS, gas-phase and aqueous basicities do not sufficiently explain analyte behaviours and there are other factors influencing the response of the compounds when analyzed in mixtures. In cases where a direct correlation between the gas-phase or aqueous basicities and mass spectral response is not apparent, it is possible that internal energy transfer during desorption results in ion fragmentation and loss of molecular ions. In addition, solution-phase intra- and intermolecular hydrogen bonding could influence

DOI: 10.1002/rcm

ionization. Further investigations will be required to understand the propensity for some ions to be detected in preference to others.

Whilst it may be possible to detect quantitative changes for individual analytes in mixtures, as demonstrated with histidine in this study (Fig. 5), ion suppression effects are operational when one analyte is allowed to dominate the rest. However, some analytes (e.g., arginine in this study) are relatively unperturbed even when one analyte (histidine here) is allowed to increasingly dominate the mixture. Clearly, there is much to be desired in our understanding of the behaviour of the analytes in mixtures to enable us to devise strategies to address such anomolies before the technique can be applied to monitor quantitative changes reliably in metabolomic investigations.

Metabolomics is a broad discipline and analyses range from monitoring changes in the levels of known metabolites, in a relatively constant biological matrix, to discovering changes in yet to be identified (potential) markers, in a varying complex biological matrix. LDI-MS on porous silicon, in its current form, can be used to monitor changes in known metabolites in a relatively simple biological matrix. When a complex milieu is analyzed, it may still be possible to apply the technique beneficially with the use of multivariate analysis to discriminate changes in response patterns detected, as demonstrated elsewhere for gene function analysis.[29] However, suitable analytical and chemometric validation steps will be needed before routine applications are possible. Clearly, further development of the technique is required before it can be used as a routine quantitative discovery tool in metabolome analyses, and further mechanistic investigations of the surface chemistry should assist in the development of strategies to overcome ion suppression effects.

Acknowledgements

The authors are grateful to Dr Roger Jarvis for help with Raman spectroscopy, Prof. Douglas Kell for useful discussions, and the Engineering and Biological Systems Committee of the BBSRC, UK, for financial assistance.

REFERENCES

1. Raamsdonk LM, Teusink B, Broadhurst D, Zhang N, Hayes A, Walsh MC, Berden JA, Brindle KM, Kell DB, Rowland JJ, Westerhoff HV, van Dam K, Oliver SG. *Nat. Biotechnol.* 2001; **19**: 45.
2. Kell DB. *Biochem. Soc. Trans.* 2005; **33**: 520.
3. Nielsen J, Oliver S. *Trends Biotechnol.* 2005; **23**: 544.
4. Vaidyanathan S. *Metabolomics* 2005; **1**: 17.
5. Vaidyanathan S, Harrigan GG, Goodacre R (eds). *Metabolome Analyses: Strategies for Systems Biology*. Springer: New York, 2005.
6. Soo EC, Aubry AJ, Logan SM, Guerry P, Kelly JF, Young NM, Thibault P. *Anal. Chem.* 2004; **76**: 619.
7. Allen J, Davey HM, Broadhurst D, Heald JK, Rowland JJ, Oliver SG, Kell DB. *Nat. Biotechnol.* 2003; **21**: 692.
8. Kaderbhai NN, Broadhurst DI, Ellis DI, Goodacre R, Kell DB. *Compar. Funct. Genom.* 2003; **4**: 376.
9. Goodacre R, Vaidyanathan S, Dunn WB, Harrigan GG, Kell DB. *Trends Biotechnol.* 2004; **22**: 245.
10. Dunn WB, Ellis DI. *Trends Anal. Chem.* 2005; **24**: 285.
11. Koek MM, Muilwijk B, van der Werf MJ, Hankemeier T. *Anal. Chem.* 2006; **78**: 1272.
12. Lafaye A, Labarre J, Tabet JC, Ezan E, Junot C. *Anal. Chem.* 2005; **77**: 2026.
13. Soga T, Ohashi Y, Ueno Y, Naraoka H, Tomita M, Nishioka T. *J. Proteome Res.* 2003; **2**: 488.
14. Maharjan RP, Ferenci T. *Anal. Biochem.* 2003; **313**: 145.
15. Bollard ME, Stanley EG, Lindon JC, Nicholson JK, Holmes E. *NMR in Biomedicine* 2005; **18**: 143.
16. Ellis DI, Goodacre R. *Analyst* 2006; **131**: 875.
17. Cohen LH, Gusev AI. *Anal. Bioanal. Chem.* 2002; **373**: 571.
18. Ayorinde FO, Hambright P, Porter TN, Keith QL Jr. *Rapid Commun. Mass Spectrom.* 1999; **13**: 2474.
19. Woldegiorgis A, von Kieseritzky F, Dahlstedt E, Hellberg J, Brinck T, Roeraade J. *Rapid Commun. Mass Spectrom.* 2004; **18**: 841.
20. Tholey A, Wittmann C, Kang MJ, Bungert D, Hollemeyer K, Heinzle E. *J. Mass Spectrom.* 2002; **37**: 963.
21. Crecelius A, Clench MR, Richards DS, Evason D, Parr V. *J. Chromatogr. Sci.* 2002; **40**: 614.
22. McCombie G, Knochenmuss R. *Anal. Chem.* 2004; **76**: 4990.
23. Vaidyanathan S, Gaskell S, Goodacre R. *Rapid Commun. Mass Spectrom.* 2006; **20**: 1192.
24. Wei J, Buriak JM, Siuzdak G. *Nature* 1999; **399**: 243.
25. Shen ZX, Thomas JJ, Averbuj C, Broo KM, Engelhard M, Crowell JE, Finn MG, Siuzdak G. *Anal. Chem.* 2001; **73**: 612.
26. Go EP, Prenni JE, Wei J, Jones A, Hall SC, Witkowska HE, Shen Z, Siuzdak G. *Anal. Chem.* 2003; **75**: 2504.
27. Go EP, Apon JV, Luo G, Saghatelian A, Daniels RH, Sahi V, Dubrow R, Cravatt BF, Vertes A, Siuzdak G. *Anal. Chem.* 2005; **77**: 1641.
28. Go EP, Shen Z, Harris K, Siuzdak G. *Anal. Chem.* 2003; **75**: 5475.
29. Vaidyanathan S, Jones D, Broadhurst DI, Ellis J, Jenkins T, Dunn WB, Hayes A, Burton N, Oliver SG, Kell DB, Goodacre R. *Metabolomics* 2005; **1**: 243.
30. Lewis WG, Shen ZX, Finn MG, Siuzdak G. *Int. J. Mass Spectrom.* 2003; **226**: 107.
31. Okuno S, Arakawa R, Okamoto K, Matsui Y, Seki S, Kozawa T, Tagawa S, Wada Y. *Anal. Chem.* 2005; **77**: 5364.
32. Kruse RA, Li XL, Bohn PW, Sweedler JV. *Anal. Chem.* 2001; **73**: 3639.
33. Alimpiev S, Nikiforov S, Karavanskii V, Minton T, Sunner J. *J. Chem. Phys.* 2001; **115**: 1891.
34. Petrova EA, Bogoslovskaya KN, Balagurov LA, Kochoradze GI. *Mater. Sci. Eng. B Solid State Materials Advanced Technology* 2000; **69**: 152.
35. Thompson WH, Yamani Z, Hassan LHA, Greene JE, Nayfeh M, Hasan MA. *J. Appl. Phys.* 1996; **80**: 5415.
36. Frotscher U, Rossow U, Ebert M, Pietryga C, Richter W, Berger MG, ArensFischer R, Munder H. *Thin Solid Films* 1996; **276**: 36.
37. Gorecka-Drzazga A, Bargiel S, Walczak R, Dziuban JA, Kraj A, Dylag T, Silberring J. *Sensors Actuators B Chemical* 2004; **103**: 206.
38. Trauger SA, Go EP, Shen Z, Apon JV, Compton BJ, Bouvier ES, Finn MG, Siuzdak G. *Anal. Chem.* 2004; **76**: 4484.
39. Luo GH, Chen Y, Siuzdak G, Vertes A. *J. Phys. Chem. B* 2005; **109**: 24450.
40. Detter LD, Hand OW, Cooks GR, Walton RA. *Mass Spectrom. Rev.* 1988; **7**: 465.
41. Sunner JA, Kulatunga R, Kebarle P. *Anal. Chem.* 1986; **58**: 1312.
42. Knochenmuss R, Zenobi R. *Chem. Rev.* 2003; **103**: 441.
43. Hunter EPL, Lias SG. *J. Phys. Chem. Ref. Data* 1998; **27**: 413.

DOI: 10.1002/rcm